



Thermal properties of multilayer graphene and hBN reinforced copper matrix composites

Marek Kostecki¹ · Tomasz Cygan¹ · Mateusz Petrus¹ · Jakub Jaroszewicz¹

Received: 27 November 2018 / Accepted: 27 April 2019 / Published online: 15 May 2019
© The Author(s) 2019

Abstract

The unique properties of graphene make it a very attractive application, although there are still no commercial products in which graphene would play a key role. Good thermal conductivity is undoubtedly one of the attributes which can be easily used both in materials involving large monoatomic layers, that are very difficult to obtain, as well as multilayer graphene flakes, which have been commercially available on the market for several years. The article presents the results of tests on the characteristic thermal properties of composites with the addition of 2–15% of multilayer graphene (MLG) crystals. The motivation of the study was literature reports showing the possibility of increasing the thermal conductivity of composites with MLG participation in the copper matrix. Since the production of composites with increased properties is associated with obtaining a strong orientation of the flakes in the structure, composites with hBN flakes exhibiting significantly worse but also directional thermal properties were produced for comparison. The paper showed a strong influence of flake morphology on the possibility of creating a directional structure. The obtained Cu/MLG composites with the addition of only 2% MLG were characterized by an increase in the thermal conductivity coefficient of about 30% in relation to sinters without the participation of MLG.

Keywords Multilayer graphene · Copper/graphene composites · Thermal conductivity

Introduction

Metals, due to the presence of metallic bonds and free-moving electrons, are good thermal conductors [1]. When seeking good thermal management, probably the first choice will be representative of this group of materials. Although this is not an obvious selection, different forms of carbon have proved to be a much better candidate.

For many decades, first place in heat transfer was taken by diamond, where uniform, continuous three-dimensional network of C–C single bonds (σsp^3) provides high thermal conductivity (TC), measured to be more than $2400 \text{ W m}^{-1} \text{ K}^{-1}$, which is almost six times more than copper [2]. However, unlike metals, heat transport in diamond is the result of elastic vibrations of the lattice (phonons).

As in the case of diamond, the thermal conductivity of graphite is mainly due to phonons. High in-plane thermal conductivity is the result of sp^2 covalent bonding between carbon atoms, but large lattice spacing in the c-direction and the weak van der Waals bonding forces between basal planes cause strong thermal anisotropy with over 100-fold between the in-plane and out-of-plane directions ($20 \text{ W m}^{-1} \text{ K}^{-1}$) [3–5]. This is a value impossible to achieve for a diamond where thin polycrystalline layers, obtained by using CVD methods, may result only about 50% differences in conductivity depending on the direction [6, 7].

✉ Marek Kostecki
marek.kostecki@pw.edu.pl

Tomasz Cygan
tomasz.cygan@pw.edu.pl

Mateusz Petrus
mateusz.petrus@pw.edu.pl

Jakub Jaroszewicz
jakub.jaroszewicz@pw.edu.pl

¹ Faculty of Materials Science and Engineering, Warsaw University of Technology, Wołoska St. 141, 02-507 Warsaw, Poland

On the one hand, anisotropy affects the low average conductivity of polycrystalline graphite, but on the other hand, the individual layers of graphite in the form of graphene [8] are characterized by a much higher in-plane thermal conductivity, whose values are up to $5300 \text{ W m}^{-1} \text{ K}^{-1}$ in room temperature [9]. Furthermore, some mathematical models indicate that it may be even larger and will grow with the increasing linear dimensions of graphene flakes [10, 11].

Such exceptional thermal properties make graphene a very desirable material. However, the complicated manufacturing process and the constantly high costs of producing monolayers make it possible to use rather as a thermal management material in future nanoelectronic circuits [12], interface materials [13, 14] or thermal phase change materials [15].

Nowadays, the possibilities of using graphene in the form of multilayered graphene (MLG) [16, 17] on a mass scale as a component of bulk composite materials with increased thermal properties are being investigated. One should take into account the fact that multilayer graphene flakes will have a lower conductivity than monolayers. It has been clearly demonstrated that increasing the number of graphene layers will cause a decrease in in-plane thermal conductivity due to the cross-plane coupling of phonons, which was induced by the van der Waals forces between the layers [18, 19]. However, the stronger this argument is, all potential materials constituting a possible matrix will have a much lower TC, and obstacles to obtaining good properties of composite should be looked for elsewhere.

The problem to take into account is the graphene itself; isotopes, strain, chemical functionalization [10] and defects [20] can lead to considerable reduction in graphene TC. An even more important issue is related to the effect of bonding on phonon transmission and thermal boundary conductance (TBC) at the interface. For example, TBC across Cu/single-layer graphene interfaces is about $10 \text{ MW m}^{-2} \text{ K}^{-1}$ [21] which is 1–3 order of magnitude lower than in pure metal [22], whereas the interfacial conducts between metal and c-axis for highly oriented pyrolytic graphite (HOPG) are similar to those of metals and diamond [23]. This fact is a huge obstacle in the production of composites based on metals with increased properties in which the effect of high in-plane conductivity of graphene can be used [24].

The analysis of the literature concerning both numerical simulations and real materials produced by different techniques suggests that important parameters which allow improvement in thermal properties to be achieved lie mainly in the precise planning of the composite microstructure [25]. Although the task is technologically difficult, it turns out to be a solution to the problems described earlier.

One of the first works in which the improvement in composite properties was achieved concerned the orientation of graphene flakes. Thermal conductivity of electrochemically deposited Cu/graphene composite films was increased to $460 \text{ W m}^{-1} \text{ K}^{-1}$. It was found that the cross-plane thermal conductivity is reduced as a result of the low thermal conductivity of graphene perpendicular to the planes, although the interface thermal resistance was not a limiting factor [26]. Instead, the smaller size of graphene platelets is thought to be the limitation [27].

Other studies carried out for bulk composites also indicate the possibility of a significant increase in conductivity under the condition of manufacturing high degree of alignment of graphite nanoplatelets, and the use of flakes of the largest possible lateral size [28]. The same authors soon developed a composite with in-plane thermal conductivity of $503 \text{ W m}^{-1} \text{ K}^{-1}$ and ultralow thermal expansion, where graphite platelets have lateral size of $300 \mu\text{m}$ and $5 \mu\text{m}$ thickness [29].

Very similar conclusions were drawn by the authors of subsequent works indicating increased thermal properties of composites containing just “fine graphite flakes” instead of graphene. Electroless plating of copper on the graphite flake and further SPS (spark plasma sintering) of composite powders allowed the obtaining of composites with 44–71 vol% flakes, which exhibit excellent thermophysical properties. TC of the composites increases from 445 to $565 \text{ W m}^{-1} \text{ K}^{-1}$, and the coefficient of thermal expansion (CTE) decreases almost 40%. Composites exhibited adaptive thermal properties which can be adjusted with the volume ratio of the graphite flakes [30]. Vacuum hot-pressed composites with increasing volume fraction of graphite flakes from 40 to 70% showed the in-plane thermal conductivity (perpendicular to the pressing direction) increase from 474 to $676 \text{ W m}^{-1} \text{ K}^{-1}$ [31]. Although composites with such a large amount of graphite may be desirable due to functional properties, it is expected that the mechanical properties will deteriorate [32]. One of the most recent works indicates very good effects of the use of the vacuum filtration process in obtaining the highly aligned graphene nanoplatelet (GNP) network. Composites with a GNP share of 35 vol% were characterized by TC at $525 \text{ W m}^{-1} \text{ K}^{-1}$ [33].

In order to summarize the previous consideration, it should be stated that a well-bonded interface and good alignment in the metal matrix composites is the key to efficient TC improvement [34]. Other important factors are graphene lateral size and thickness which can be considered as “relatively large.” The assessment of the impact of the volume share and percolation effect [35] is still unclear because an improvement was obtained for composites containing 20 to 70 vol%, and in each case the dispersion and alignment were the most important issue.

The available study clearly formulates the rules required to achieve elevated but highly directional thermal properties. Although in most of the previously presented research the applied production methods are quite sophisticated, authors of this article decided to use a simple SPS technique. SPS favors the self-alignment of graphene platelets due to the use of axial pressing [36]. Particular attention was paid to the morphology of the particles. In previous works [37], it was found that in the SPS method the morphology of the 2D particles is of great importance in shaping the microstructure. Therefore, composites with the addition of other 2D crystals, like hexagonal boron nitride (hBN), representing a different morphology were made for comparison. For thin hBN flakes, the in-plane thermal conductivity could exceed, or be comparable to, that of its bulk crystalline ($\sim 390 \text{ W m}^{-1} \text{ K}^{-1}$) [38]. Although hBN is not a competition for carbon flakes, similarly to MLG, they have a strong anisotropy of thermal properties. Unlike MLG, hBN is also an excellent electrical insulator which can be used, where electrical insulation is required [39, 40] together with high TC. For both types of composites containing 2 to 15% by volume of MLG or hBN particles, the microstructure was investigated and its influence on thermal properties was determined.

Materials and methods

In order to produce two series of copper/graphene and copper/hBN composites, with the contents of the second phase of 0, 2, 5, 10 and 15% by volume, the following powders were used: *copper* powder produced by Acros Organics, a purity of 99.5%, an average particle size of $32 \mu\text{m}$ (Fig. 1a), *MLG* powder, trade name Gn (12) produced by Graphene Supermarket USA, with an average flake thickness of 12 nm and average lateral size of $4.5 \mu\text{m}$ (Fig. 1b) and *hBN* powder from MK Impex Corp, trade name N70, flake average thickness 70 nm and average lateral size 570 nm (Fig. 1c).

After weighing, the powder mixtures were homogenized in a rotational horizontal mill in the presence of alumina ceramic balls (with balls-to-powder ratio 6:1) and isopropyl alcohol for 8 h. The rotational speed has been selected at 300 rpm enabling the smallest number of defects to be introduced into layered crystals. Dried powder was granulated on # 0.3-mm sieves.

Synthesis of composites was carried out in the spark plasma sintering process using the SPS HP D10 device (FCT Systeme GmbH, Rauenstein, Germany), in accordance with the proposed parameters: sintering temperature $T = 850 \text{ }^\circ\text{C}$, atmosphere—argon at reduced pressure, sintering time $t = 4 \text{ min}$ and pressure $p = 50 \text{ MPa}$. Temperature and process time were optimized toward the highest

relative density without melting the metallic matrix. Pressure selection was the result of limitations related to the strength of graphite matrices with a diameter of 20 mm.

The obtained sinters in the form of a cylinder with a diameter of 20 mm and a height of 15 mm were cleaned and fragmented for specific tests. A minimum of three samples cut from a representative area in three different sinters were prepared for one test. A high-speed saw with a diamond blade (under cooling conditions) was used to avoid microstructural changes.

As a result of SPS, alignment of the flakes in the structure of composites has been observed which will be described at the stage of analysis of the microstructure. This alignment is consistent with the axis of the sample determined in the direction perpendicular to the pressing direction; therefore, measurement of properties has been made perpendicular or parallel to this direction as well as procedure of sample cutting (Fig. 2).

The powders' morphology and microstructure were observed using scanning electron microscopes (Hitachi S5500, Japan). Microcomputed tomography (Zeiss Xradia MicroXCT-400) was performed on the composites structure, to illustrate the agglomerates geometry and aligning. The obtained resolution was $10 \mu\text{m}$. The scanning procedure was carried out by performing a rotation of the emitted X-ray by 180° , with a step size of 0.15° and an exposure time of 15 s per projection. Density tests were carried out using the helium pycnometer (Ultracycrometer 1000, Quantachrome Instruments) for bulk sinters cleaned from graphite foil. Calorimetric measurements (DSC) were carried out to determine the specific heat (C_p). Two series of randomly oriented cuboidal samples with dimensions $1 \times 1 \times 0.5 \text{ mm}$ were measured using Netzsch, STA 449 F5 Jupiter. The thermal diffusivity (D) was measured at room temperature by a laser flash method, using LFA 457,

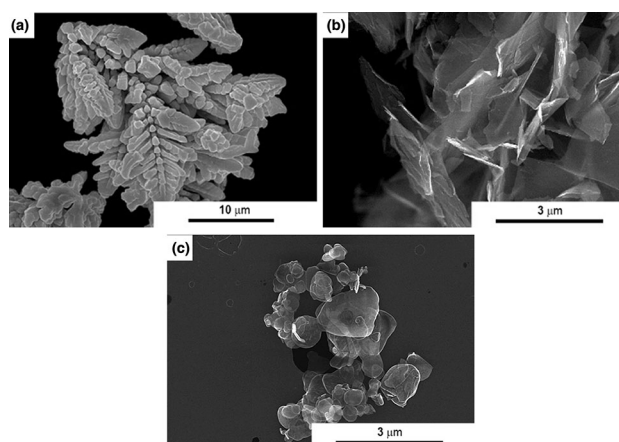
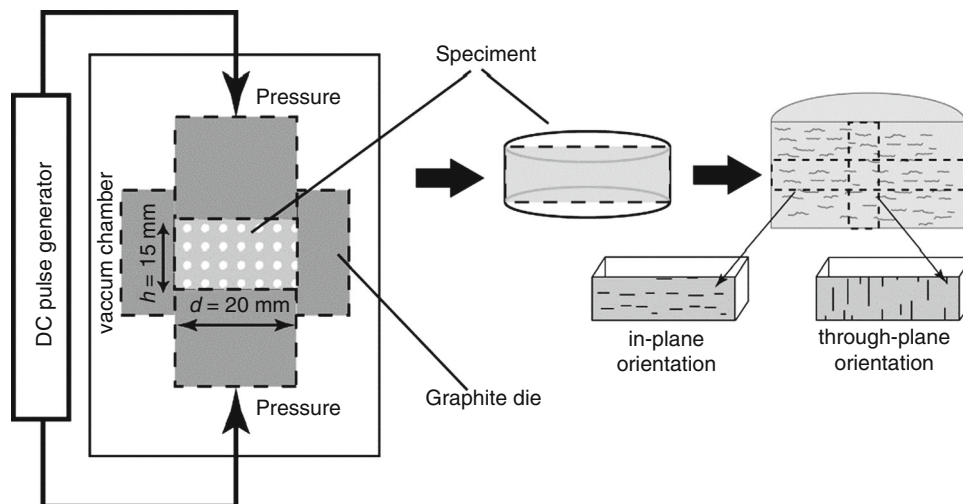


Fig. 1 Morphology of **a** Cu powder, **b** MLG powder and **c** hBN powder (SEM images)

Fig. 2 Composites preparation and sample cutting procedure



Netzsch. Measurements were made for two series of cuboidal samples with dimensions of $8 \times 8 \times 3 \text{ mm}$ in the direction parallel and perpendicular to pressing direction. Mathematical analysis of the phenomenon implemented in the software takes into account the improved Cape–Lehman model. The standard deviation of measurements in the case of Cp and D was within 3%, and error bars in most cases are in size of measure points. The thermal expansion coefficient was measured using Netzsch DIL 402 Expedit Classic a vertical direct dilatometer. Cuboid samples were used ($3 \times 3 \times 12 \text{ mm}$) with different reinforcement alignment: parallel and perpendicular to pressing direction. The samples were heated up to the temperature of $500 \text{ }^\circ\text{C}$ in a protective atmosphere (argon flow rate $50 \text{ ml}\cdot\text{min}^{-1}$) at a rate of $5 \text{ }^\circ\text{C}\cdot\text{min}^{-1}$. The values of the thermal expansion coefficient were determined based on the measurements of the elongation of the samples as a function of the temperature $\alpha = (\Delta l \cdot l_0^{-1}) \cdot \Delta T$. All measurements of thermal properties were carried out at a temperature range $20\text{--}500 \text{ }^\circ\text{C}$.

Results and discussion

It can be observed that graphene flakes are not “linked” to dendrites of copper powder particles which, under the influence of the mixing, have undergone a slight deformation (flattening). Much smaller flakes of hexagonal boron nitride seem to be “glued” to the copper particles and also localized in copper dendrites open spaces (Fig. 3b). In fact, they are stuck in soft copper at the stage of ball collisions, contributing to a better dispersion of hBN particles.

However, increasing the volume of the hBN in the mixture can promote their agglomeration because the small plates have the ability to fill the porous structure better, the

more they are in the volume. It can also be assumed that with the same volume fraction of both powders, a much larger contact surface will occur in the case of hBN particles.

Density

The use of the SPS technique makes it possible to obtain sinters with a high density exceeding 90% relative density within an extremely short sintering time ($t = 4 \text{ min.}$), even at a high volume fraction of the additive.

Very good results in the intensification of the compaction process are given by its modification taking into account additional plastic deformation [41]; however, in the case of the designed properties it would be unjustified because it may lead to destruction of alignment. Figure 4 presents the graph of relative density dependence on the content of the second phase. The highest values of relative density (99.8%), close to the theoretical density, were obtained for copper sinters without additives. Composites are characterized by an almost linear decrease in density with an increase in the volume fraction of the second phase. Relative density obtained for MLG composites is lower than for hBN in the whole range of compositions and for 15% of the additive falls slightly below 94%. Density decrease is a typical situation for composites manufactured by the powder metallurgy processes where nanometric powders are responsible for strong agglomeration. The porosity can be observed in the microstructure, which is described further.

Microstructure

SEM observations were carried out using cross section specimens. Samples for observation were oriented so that the long edge of the drawing is perpendicular to the axis

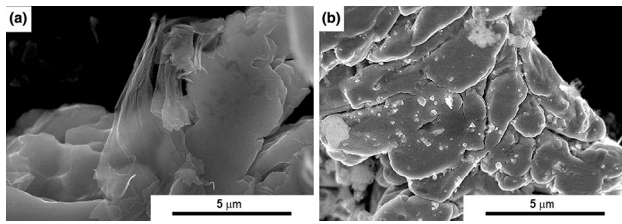


Fig. 3 Morphology of mixed powders: **a** Cu + 10 vol% MLG powder and **b** Cu + 10 vol% hBN powder (SEM images)

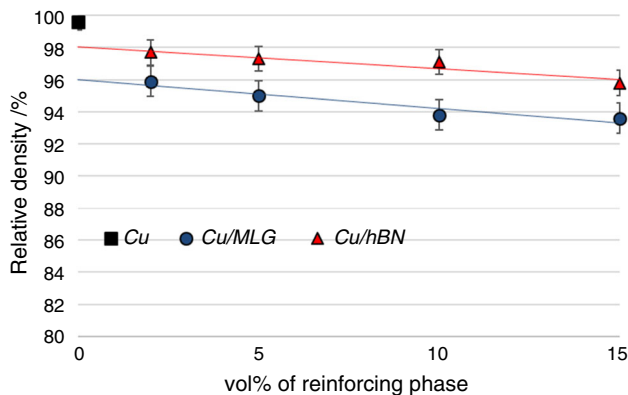


Fig. 4 Relative density of Cu/MLG and Cu/hBN composites obtained in SPS process

that determines the direction of the force in the SPS process. It can be observed that the MLG agglomerates are perpendicular to the direction of pressure applied during the process (Fig. 5). The average thickness of the agglomerate bands varies with the volume fraction of MLG flakes from 1.5 μm for 2 vol% to 3.8 μm for 15 vol%. The agglomerates seen in Fig. 5c indicate the primary source of porosity. As can be seen, the obtained porosity is mainly the result of insufficient space filling by layered crystals which, through their morphology and the fact of the presence on the boundaries of irregular Cu powder particles, generate a large amount of nanopores. It cannot be unambiguously determined whether there is percolation of phases in the composite.

Composites with the addition of hBN flakes present a slightly different structure (Fig. 6). The smaller hBN flakes already at the mixing process were located in the interstices of the dendritic structure of the copper particles, resulting in better dispersion. In 2 vol% composites, agglomerates are equi-axial and have no specific orientation; the exception are packets of flakes created during mixing consisting of several to several dozen plates connected along basal planes (Fig. 6c). Porosity is observed similarly to MLG mainly within the agglomerates. The shape of these agglomerates differs from those observed in the MLG composites; moreover, their size and shape change with an

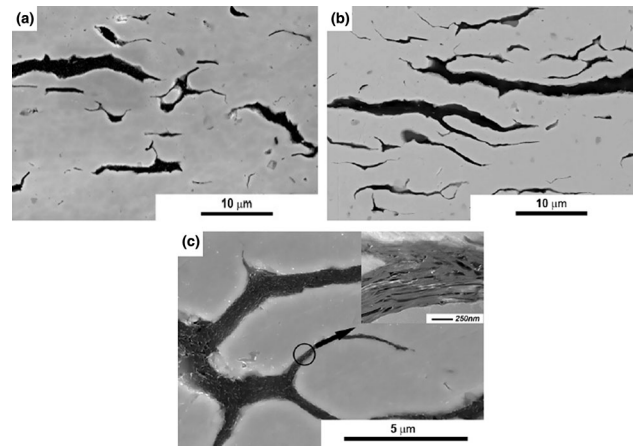


Fig. 5 Microstructure of composites: **a** Cu + 2 vol% MLG, **b** Cu + 10 vol% MLG and **c** Cu + 10 vol% MLG (SEM images except enlarged area of the MLG agglomerate—TEM image)

increase in the volume fraction of hBN flakes. Addition of 10 vol% hBN creates bands (in three-dimensional space these are disks) with a length of a dozen or so micrometers. Observation of randomly oriented images in relation to the direction of the compaction process indicates that there is no clear orientation of the hBN agglomerates (Fig. 6b).

Because the cross section observation at high magnification does not provide sufficient information about the hBN agglomerates, CT scans were performed and 3D structure images describing spatial distribution were prepared with resolution down to 10 μm (Fig. 7).

The resolution was applied due to isolation of the largest agglomerates in a relatively large sample volume. In these conditions, due to a number of smaller particles the use of higher resolution would render the images illegible.

The analysis shows that in the volume of material, especially in the case of composites with hBN (Fig. 7b), apart from the previously indicated fine agglomerates, there are also objects with dimensions exceeding 10 μm whose orientation is similar to that represented by elongated agglomerates of MLG. The mean value of the slope angle of the longer axis of these objects relative to the pressure force is 89.3° , while for agglomerates MLG is 90.4° , so one can say that their orientation is very similar and almost perpendicular to the pressing direction (Fig. 8).

We can therefore assume that we also deal with a composite with an anisotropic structure. However, from the point of view of essential thermal properties, the anisotropy of large agglomerates should not translate into anisotropy of properties because the flakes inside them can be set quite by accident (Fig. 6c). In the case of MLG, the alignment takes place at the level of individual flakes as well as in the case of agglomerates.

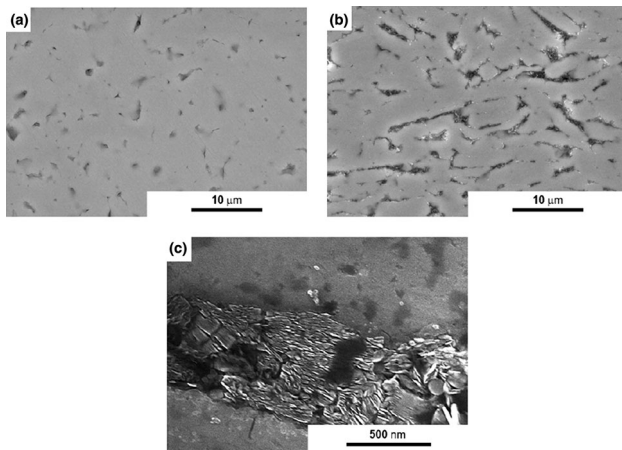


Fig. 6 Microstructure of composites: **a** Cu + 2 vol% hBN, **b** Cu + 10 vol% hBN and **c** Cu + 10 vol% hBN—area of the hBN agglomerate (SEM images)

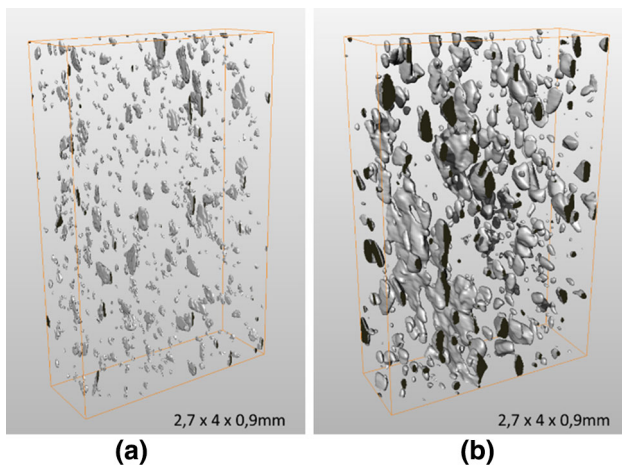


Fig. 7 Three-dimensional structure of **a** Cu/10 vol% MLG and **b** Cu/10 vol% hBN composites

Specific heat capacity

Specific heat capacity of composite materials is an essential parameter, especially in the determination of thermal conductivity. Because this property is independent of the structure, it was measured for randomly cut samples without selecting a specific direction [42].

Most specific heat capacity values of composites at different filler contents are normally obtained by using the rule of mixture when the heat capacities of the filler and the matrix are known. However, utilization of differential scanning calorimetry techniques in this case is more accurate. Literature data indicate room-temperature specific heat for graphite is $C_p \approx 0.850 \text{ J g}^{-1} \text{ K}^{-1}$ [43], for hBN it is very similar $C_p \approx 0.780 \text{ J g}^{-1} \text{ K}^{-1}$ [44] and for copper it is $C_p \approx 0.385 \text{ J g}^{-1} \text{ K}^{-1}$ [45]. While in the case

of hBN composites the measured values obtained agree well with the calculations, in the case of MLG composites they are about $0.1 \text{ J g}^{-1} \text{ K}^{-1}$ higher (Fig. 9a). The reason for raising the specific heat of the composite may lie in the graphene flakes themselves, for which the strain will affect the actual value of this property [46]. At the same time, it is known that the SPS process can generate a large number of stress and strain in the material structure. For the full analysis of the problem, one should carry out studies of residual stresses in the composite taking into account: parameters of the microstructure, type of layered crystals, the porosity and the possibility of stress relaxation with increasing temperature.

In the case of both types of composites, the obtained specific heat capacity values are higher than for copper sinters and slightly dependent on the volume fraction of the additive. The C_p increases with the increase in the volume share of the additive which is noticeable.

Thermal diffusivity

The first strong directional relationship is visible for the examined composites in thermal diffusivity measurements. Figure 10a, b shows diagrams of diffusivity versus temperature for composites with different MLG content. Measurements for the barrier direction (through-plane) indicate that the addition of MLG greatly weakens the heat flow rate. The value decreases when more MLG is added, and in the case of 15% in volume the value causes a fivefold decrease in diffusivity. Measurements for a sample oriented toward good heat conduction indicate a slight decrease in diffusivity with the increase in MLG content. With the 15 vol% decrease is about 18% (Fig. 10a).

Despite the lack of a pronounced orientation of the flakes (not agglomerates) in the hBN composites, changes in the heat flow rate associated with the volume fraction of the powder are similar to those represented by the MLG composites (Fig. 11). While the values measured in the perpendicular direction are very close to the MLG composites (Fig. 11b), decrease in diffusivity in the direction parallel to the pressure force is lower than for MLG (Fig. 11a). There is no proportional drop in diffusivity when increasing the volume of hBN. Up to 10% of flakes, the decrease is about 27%, while for 15% of flakes the fall is considerable, about 55%. This observation allows one to suppose that some aligning in global scale has occurred and becomes significant for the higher volume fraction of hBN particles. The microstructure analysis shows that for those composites, there are bands that can significantly block the flow of heat in a direction parallel to the pressure, and thus a larger number of flakes within the bands are aligned. The second observation is related to the flow toward easy conduction direction (in-plane). We can say that despite the

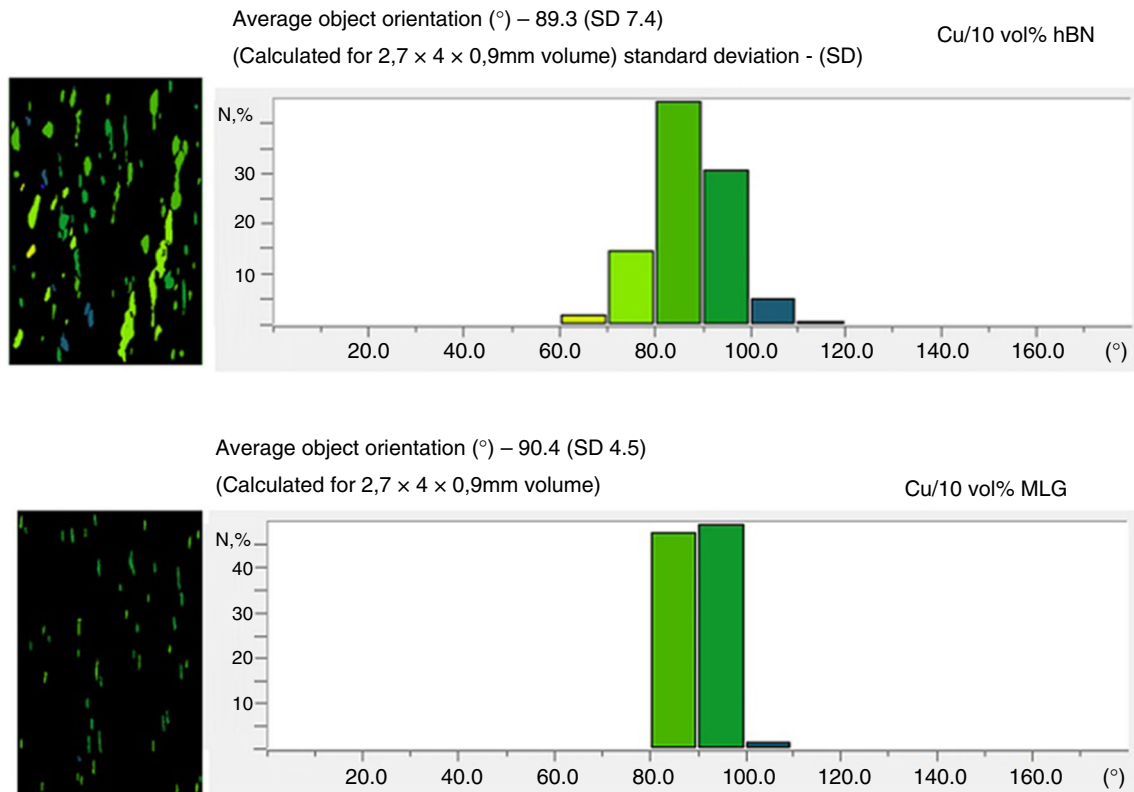


Fig. 8 Example of 2D color image highlights the different orientations of the objects and histogram showing the distribution of orientations

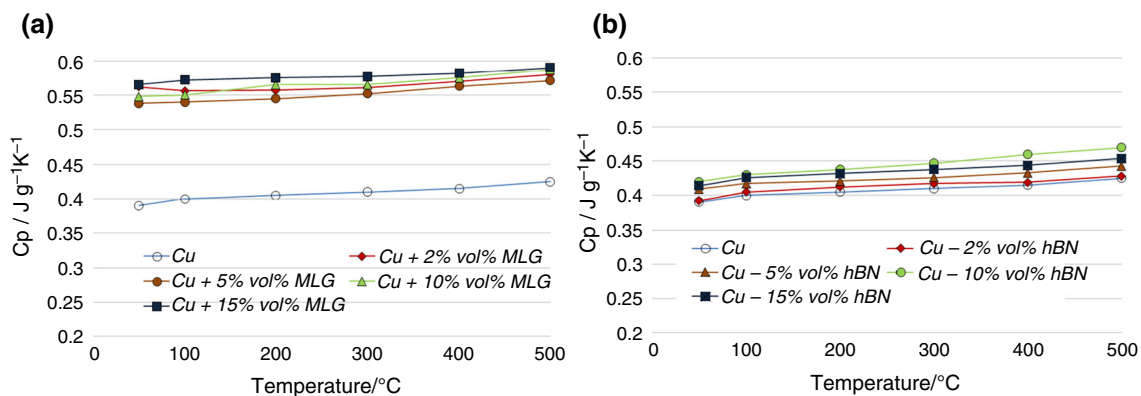


Fig. 9 Specific heat of **a** Cu/MLG and **b** Cu/hBN composites

use of particles with a different morphology and significantly different thermal properties, there is no difference in the heat flow rate, which may suggest a great contribution of copper to the value of this parameter in the composites, where addition is in the range of 2–15 vol%.

Thermal expansion coefficient

Copper is a metal with a relatively high coefficient of thermal expansion, which often causes problems in the

design and use of composites on its matrix, especially when the second phase is ceramic materials. An additional problem may be wettability affecting the nature of the interface as in diamond composites [47]. The conducted dilatometer tests indicate (Fig. 12) that for the obtained composites thermal expansion is also a property dependent on the direction of measurement. The observed anisotropy is small. Cu sinters have a CTE value of $17.8 \cdot 10^{-6} \text{ K}^{-1}$, which is a slightly higher than given in the literature for pure metallurgical copper $17 \cdot 10^{-6} \text{ K}^{-1}$ [48]. The

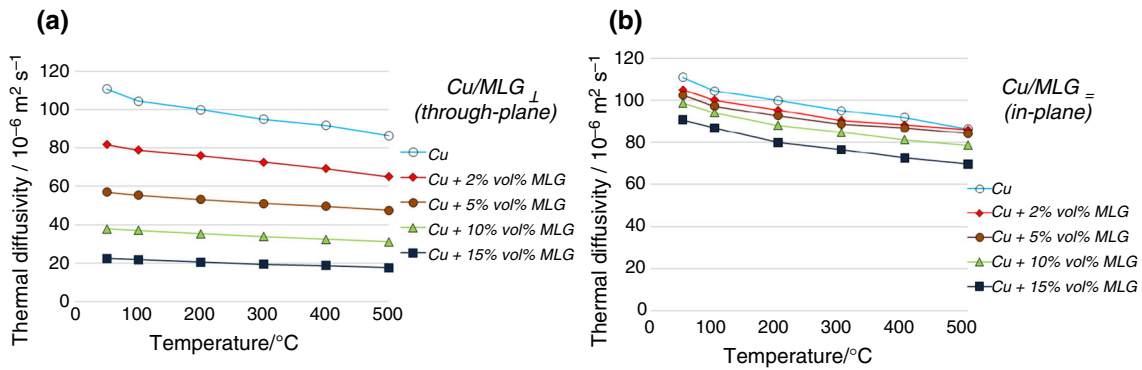


Fig. 10 Thermal diffusivity as a function of temperature for Cu/MLG composites **a** through-plane direction, **b** in-plane direction

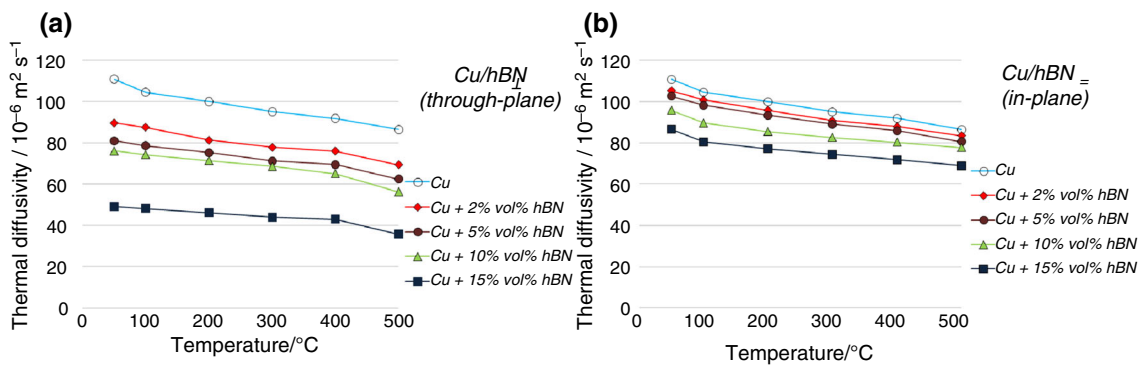


Fig. 11 Thermal diffusivity as a function of temperature for Cu/hBN composites **a** through-plane direction, **b** in-plane direction

measurements indicate that thermal expansion in MLG composites measured in the in-plane direction (perpendicular to the pressure force) is slightly lower $16.5 \cdot 10^{-6} \text{ K}^{-1}$ when sintered without additives. When measured in the direction parallel to the pressure force (through-plane), it is a bit higher $18.5 \cdot 10^{-6} \text{ K}^{-1}$. It is difficult to talk about a clear upward or downward tendencies related to the volume fraction of the addition. In the case of hBN composites, the addition of flakes reduces the coefficient of thermal expansion regardless of the direction of measurement. The results obtained are in accordance with the previously described in the literature [29], where thermal expansion coefficient does not change dramatically until the 20 vol% of graphite platelets has been exceeded.

Thermal conductivity

The experimental results of the thermal diffusivity and the specific heat were used to estimate the thermal conductivity λ . It can be determined from the relation:

$$\lambda = \rho C_p D [\text{W m}^{-1} \text{ K}^{-1}], \quad (1)$$

where λ is the thermal conductivity, ρ is the density, C_p is the specific heat, and D is the diffusivity.

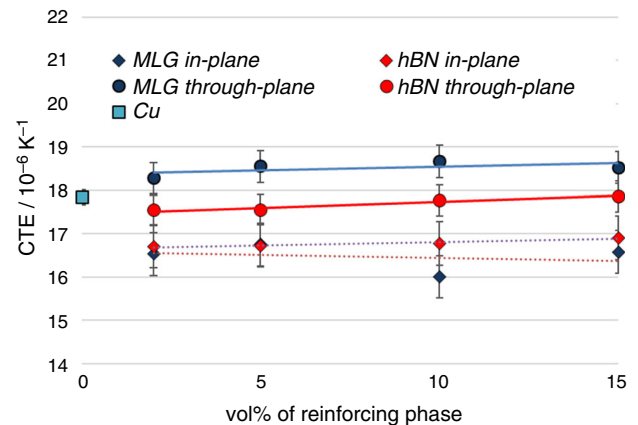


Fig. 12 Thermal conductivity of Cu/MLG and Cu/hBN composites at 50 °C

Figure 13 presents the results of thermal conductivity calculations. Analysis of the graph indicates a much stronger anisotropy of properties for the composite with the addition of MLG. Looking at the conductivity values (in-plane and through-plane measurements direction), one can clearly see that the differences increase with an increasing

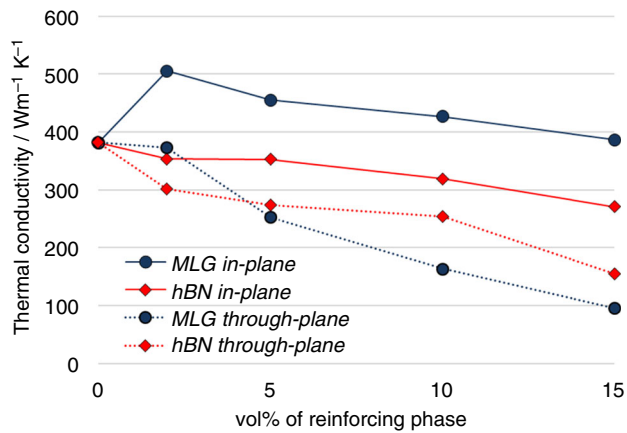


Fig. 13 Linear coefficient of thermal expansion (CTE) for Cu/MLG and Cu/hBN composites at 50 °C

volume fraction of the second phase. This tendency is not retained for composites with hBN particles, and larger differences in the thermal conductivity are visible only at the high volume fraction of the additive at the level of 15%.

In the case of the composite with 2 vol% MLG, a clear improvement in thermal conductivity of $505 \text{ W m}^{-1} \text{ K}^{-1}$ (in-plane direction) was obtained, which means an increase of 32% in relation to pure copper sinters $381 \text{ W m}^{-1} \text{ K}^{-1}$. Further increases in the volume share of MLG flakes leads to a decrease in thermal conductivity, although its value in the whole range of compositions is higher than for a sinter that does not contain graphene. An important problem may be quite high porosity of composites with a higher content of MLG (about 6% for the composite with the addition of 15 vol% MLG). This porosity will affect both the limitation of heat flow and the deterioration in mechanical properties of the obtained composites.

In the case of composite with the addition of hBN, thermal conductivity was not expected to increase. The obtained λ values in the entire range of compositions indicate a decrease in conductivity in relation to Cu sinters regardless of the direction of measurement, which is the result of low thermal conductivity of the hBN itself, but also the absence of a clear orientation of the flakes in the microstructure. However, the conducted research showed that the macroscopic bands created during the SPS synthesis cause some anisotropy of thermal properties.

Conclusions

MLG-reinforced composites have potential as directional heat dissipation materials. The SPS process provides good orientation of MLG flakes perpendicular to the direction of force, which is related to their morphology. The tests

carried out proved that a small amount of flakes (2%) has a relatively strong effect, increasing thermal conductivity of composite by 32% (in direction perpendicular to the pressing force). The value of specific heat for graphene in the presence of stress seems to be additional reason for the increase in thermal conductivity. The present literature studies do not take into account this effect analyzing specific heat of composites. For a full analysis of the problem, one should carry out studies of residual stresses in the series of composite materials.

The methods used to achieve increased thermal properties are neither costly nor requiring many technological treatments. Literature data indicate that with a large content of flakes in the volume, the enhancement of thermal properties may be higher; however, such material will be characterized by significant decreases in mechanical properties which may limit its application in structural elements.

hBN flakes with unlike morphology are characterized by a poor orientation inside agglomerates, and those agglomerates assume different shapes which translates into a smaller morphological anisotropy but also a decrease in conductivity toward direction perpendicular to the applied force. CT scans have proven that large agglomerates are formed in the volume of composites and their orientation is similar to that obtained in MLG composites.

In order to further improve the thermal properties, it is required to optimize the manufacturing process both at the sintering stage and at the homogenization stage of the powders. While the effect of morphology of 2D crystal particles is very clear, the morphology of the copper particles, which can also be optimized, remains an open question. It can be suggested that there is an optimal particle morphology that allows the best orientation. The selection of the morphology of the starting materials to obtain an appropriate microstructure should therefore be another criterion taken into account in the technological process.

Acknowledgements We would like to thank Prof. Andrzej Olszyna for substantive care and support for our research.

Open Access This article is distributed under the terms of the Creative Commons Attribution 4.0 International License (<http://creativecommons.org/licenses/by/4.0/>), which permits unrestricted use, distribution, and reproduction in any medium, provided you give appropriate credit to the original author(s) and the source, provide a link to the Creative Commons license, and indicate if changes were made.

Authors' Contributions Marek Kostecki was responsible for planning the experiments, writing the article and analyzing the data. Tomasz Cygan performed the SPS experiments. Mateusz Petrus contributed to material preparation and SEM observations. Jakub Jaroszewicz contributed to computed tomography measurements.

Funding This research was funded by National Science Centre (Grant No. UMO-2014/15/D/ST8/02643).

References

1. Tritt TM. Thermal conductivity: theory, properties, and applications. Boston: Springer; 2005. p. 21–4. <https://doi.org/10.1007/b136496>.
2. Graebner JE. Thermal conductivity of diamond. In: Pan LS, Kania DR, editors. Diamond: electronic properties and applications. Boston: Springer; 1995. https://doi.org/10.1007/978-1-4615-2257-7_7.
3. Klemens PG, Pedraza DF. Thermal conductivity of graphite in the basal plane. Carbon. 1994;32(4):735–41. [https://doi.org/10.1016/0008-6223\(94\)90096-5](https://doi.org/10.1016/0008-6223(94)90096-5).
4. Balandin AA. Thermal properties of graphene and nanostructured carbon materials. Nat Mater. 2011;10:569–81.
5. Pop E, Varshney V, Roy AK. Thermal properties of graphene: fundamentals and applications. MRS Bull. 2012;37(12):1273–81. <https://doi.org/10.1557/mrs.2012.203>.
6. Graebner JE, Jin S, Kammloft GW, Bacon B, Seibles L. Anisotropic thermal conductivity in chemical vapor deposition diamond. J Appl Phys. 1992;71:5353. <https://doi.org/10.1063/1.350553>.
7. Yamamoto Y, Imai T, Tanabe K, Tsuno T, Kumazawa Y, Fujimori N. The measurement of thermal properties of diamond. Diam Relat Mater. 1997;6(8):1057–61.
8. Novoselov KS, Geim AK, Morozov SV, Jiang D, Zhang Y, Dubonos SV, Grigorieva I, Firsov AA. Electric field effect in atomically thin carbon films. Science. 2004;306:666–9.
9. Balandin AA, Ghosh S, Bao W, Calizo I, Teweldebrhan D, Miao F, Lau CN. Superior thermal conductivity of single-layer graphene. Nano Lett. 2008;8(3):902–7. <https://doi.org/10.1021/nl0731872>.
10. Nika DL, Ghosh S, Pokatilov EP, Balandin AA. Lattice thermal conductivity of graphene flakes: comparison with bulk graphite. Appl Phys Lett. 2009;94:203103. <https://doi.org/10.1063/1.3136860>.
11. Fugallo G, Cepellotti A, Paulatto L, Lazzeri M, Marzari N, Mauri F. Thermal conductivity of graphene and graphite: collective excitations and mean free paths. Nano Lett. 2014;14:6109–14. <https://doi.org/10.1021/nl502059f>.
12. Ghosh S, Calizo I, Teweldebrhan D, Pokatilov EP, Nika DL, Balandin AA, Bao W, Miao F, Lau CN. Extremely high thermal conductivity of graphene: prospects for thermal management applications in nanoelectronic circuits. Appl Phys Lett. 2008;92(15):151911. <https://doi.org/10.1063/1.2907977>.
13. Amini S, Garay J, Liu G, Balandin AA, Abbaschian R. Growth of large-area graphene films from metal-carbon melts. J Appl Phys. 2010;108:094321. <https://doi.org/10.1063/1.3498815>.
14. Khan SMF, Balandin AA. Thermal properties of graphene and multilayer graphene: applications in thermal interface materials. Solid State Commun. 2012;152:1331–40.
15. Renteria JD, Nika DL, Balandin AA. Graphene thermal properties: applications in thermal, management and energy storage. Appl Sci. 2014;4:525–47. <https://doi.org/10.3390/app4040525>.
16. Bianco A, et al. All in the graphene family—a recommended nomenclature for two-dimensional carbon materials. Carbon. 2013;65:1–6. <https://doi.org/10.1016/j.carbon.2013.08.038>.
17. Ramirez S, Chan K, Hernandez R, Recinos E, Hernandez E, Salgado R, Khitun AG, Garay JE, Balandin AA. Thermal and magnetic properties of nanostructured densified ferrimagnetic composites with graphene—graphite fillers. Mater Des. 2017;118:75–80. <https://doi.org/10.1016/j.matdes.2017.01.018>.
18. Ghosh S, Bao W, Nika DL, Subrina S, Pokatilov EP, Lau CN, Balandin AA. Dimensional crossover of thermal transport in few-layer graphene. Nat Mater. 2010;9:555.
19. Wei Z, Ni Z, Bi K, Chen M, Chen Y. In-plane lattice thermal conductivities of multilayer graphene films. Carbon. 2011;49:2653–8. <https://doi.org/10.1016/j.carbon.2011.02.051>.
20. Gao Y, Jing Y, Liu J, Li X, Meng Q. Tunable thermal transport properties of graphene by single-vacancy point defect. Appl Therm Eng. 2017;113:1419–25. <https://doi.org/10.1016/j.applthermaleng.2016.11.160>.
21. Chen L, Huang Z, Kumar S. Impact of bonding at multi-layer graphene/metal interfaces on thermal boundary conductance. RSC Adv. 2014;4:35852–61. <https://doi.org/10.1039/C4RA03585B>.
22. Gundrum BC, Cahill DG, Averback RS. Thermal conductance of metal-metal interfaces. Phys Rev. 2006;B72:35011. <https://doi.org/10.1103/PhysRevB.72.245426>.
23. Schmidt AJ, Collins KC, Minnich AJ, Chen G. Thermal conductance and phonon transmissivity of metal–graphite interfaces. J Appl Phys. 2010;107:104907. <https://doi.org/10.1063/1.3428464>.
24. Wejrzanowski T, Grybczuk M, Wasiluk M, Kurzydowski KJ. Heat transfer through metal-graphene interfaces. AIP Adv. 2015;5:077142. <https://doi.org/10.1063/1.4927389>.
25. Wejrzanowski T, Grybczuk M, Chmielewski M, Pietrzak K, Kurzydowski KJ, Strojny-Nedza A. Thermal conductivity of metal-graphene composites. Mater Des. 2016;99:163–73.
26. Jagannadham K. Orientation dependence of thermal conductivity in copper-graphene composites. J Appl Phys. 2011;110:074901.
27. Jagannadham K. Thermal conductivity of copper-graphene composite films synthesized by electrochemical deposition with exfoliated graphene platelets. Metall Mater Trans B. 2012;43:316. <https://doi.org/10.1007/s11663-011-9597-z>.
28. Boden A, Boerner B, Kusch P, Firkowska I, Reich S. Nanoplatelet size to control the alignment and thermal conductivity in copper–graphite composites. Nano Lett. 2014;14(6):3640–4. <https://doi.org/10.1021/nl501411g>.
29. Firkowska I, Boden A, Boerner B, Reich S. The origin of high thermal conductivity and ultralow thermal expansion in copper–graphite composites. Nano Lett. 2015;15:4745–51. <https://doi.org/10.1021/acs.nanolett.5b01664>.
30. Liu Q, He X, Ren S, Zhang C, Ting-Ting L, Qu X. Thermo-physical properties and microstructure of graphite flake/copper composites processed by electroless copper coating. J Alloys Compd. 2014;587:255–9. <https://doi.org/10.1016/j.jallcom.2013.09.207>.
31. Zhu Y, Bai H, Xue C, Zhou R, Xu Q, Tao P, Wang C, Wang J, Jiang N. Thermal conductivity and mechanical properties of a flake graphite/Cu composite with a silicon nanolayer on a graphite surface. RSC Adv. 2016;6:98190. <https://doi.org/10.1039/c6ra17804a>.
32. Chu K, Wang F, Wang X, Huang D. Anisotropic mechanical properties of graphene/copper composites with aligned graphene. Mater Sci Eng A. 2018;713:269–77.
33. Chu K, Wang X, Wang F, Li Y, Huang D, Li H, Ma W, Liu F, Zhang H. Largely enhanced thermal conductivity of graphene/copper composites with highly aligned graphene network. Carbon. 2018;127:102–12. <https://doi.org/10.1016/j.carbon.2017.10.099>.
34. Chu K, Wang X, Li Y, Huang D, Geng Z, Zhao X, Liu H, Zhang H. Thermal properties of graphene/metal composites with aligned graphene. Mater Des. 2018;140:85–94. <https://doi.org/10.1016/j.matdes.2017.11.048>.
35. Kargar F, Barani Z, Lewis JS, Debnath B, Salgado R, Aytan E, Lake R, Balandin AA. Thermal percolation threshold and thermal

- properties of composites with graphene and boron nitride fillers. *ACS Appl Mater Interfaces*. 2018;10(43):37555–65.
36. Rutkowski P, Kata D, Jankowski K, Piekarczyk W. Thermal properties of hot-pressed aluminum nitride–graphene composites. *J Therm Anal Calorim*. 2015;124(1):93–100. <https://doi.org/10.1007/s10973-015-5091-1>.
 37. Wozniak J, Kostecki M, Cygan T, Buczek M, Olszyna A. Self-lubricating aluminium matrix composites reinforced with 2D crystals. *Compos B Eng*. 2017;111:1–9.
 38. Lindsay L, Broido DA. Theory of thermal transport in multilayer hexagonal boron nitride and nanotubes. *Phys Rev B*. 2012;85:035436.
 39. Zheng J, et al. High thermal conductivity of hexagonal boron nitride laminates. *2D Mater*. 2016;3:011004.
 40. Shenab H, Caiab C, Guoab J, Qianab Z, Zhao N, Xu J. Fabrication of oriented hBN scaffolds for thermal interface materials. *RSC Adv*. 2016;6:16489–94. <https://doi.org/10.1039/C6RA00980H>.
 41. Kostecki M, Petrus M, Woźniak J, Cygan T, Olszyna A. Closed die upsetting of aluminum matrix composites reinforced with molybdenum disulfide nanocrystals and multilayer graphene, implemented using the SPS process—microstructure evolution. *Materials*. 2018;11(6):994. <https://doi.org/10.3390/ma11060994>.
 42. Ishida H, Rimdusit S. Heat capacity measurement of boron nitride-filled polybenzoxazine, the composite structure-insensitive property. *J Therm Anal Calorim*. 1999;58:497–507.
 43. Tohei T, Kuwabara A, Oba F, Tanaka I. Debye temperature and stiffness of carbon and boron nitride polymorphs from first principles calculations. *Phys Rev B*. 2006;73:064304.
 44. Gorbunov VE, Gavrichev KS, Totrova GA, Bochko AV, Lazarev VB. Russian. *J Phys Chem*. 1988;62(1):9–12.
 45. Martin DL. The specific heat of copper from 20 to 300 K. *Can J Phys*. 1960;38(1):17–24. <https://doi.org/10.1139/p60-003>.
 46. Ma F, Zheng HB, Sun YJ, Yang D, Xu KW, Chu PK. Strain effect on lattice vibration, heat capacity, and thermal conductivity of graphene. *Appl Phys Lett*. 2012;101:111904.
 47. Yoshida K, Morigami H. Thermal properties of diamond/copper composite material. *Microelectron Reliab*. 2004;44(2):303–8. [https://doi.org/10.1016/S0026-2714\(03\)00215-4](https://doi.org/10.1016/S0026-2714(03)00215-4).
 48. Nix FC, MacNair D. The thermal expansion of pure metals: copper, gold, aluminum, nickel, and iron. *Phys Rev*. 1941;60:597. <https://doi.org/10.1103/PhysRev.60.597>.

Publisher's Note Springer Nature remains neutral with regard to jurisdictional claims in published maps and institutional affiliations.